Different output properties of perisomatic region-targeting interneurons in the basal amygdala

Boglárka Barsy[1], Gergely G. Szabó[1], Tibor Andrási[1,2], Attila Vikór[1] and Norbert Hájos[1]

[1]'Lendület' Laboratory of Network Neurophysiology, Institute of Experimental Medicine, Hungarian Academy of Sciences, Budapest, Hungary, [2] János Szentágothai School of Neurosciences, Semmelweis University, Budapest, Hungary

Running title: Perisomatic inputs of amygdalar principal neurons.

Contact: **Norbert Hájos**
Institute of Experimental Medicine
Hungarian Academy of Sciences
Budapest H-1450, Hungary
Phone: 36-1-2109400/387
Fax: 36-1-2109412
Email: hajos@koki.hu

Number of pages: 22
Number of figures: 5
Number of tables: 2
Number of words for Abstract: 244
Number of words for Introduction: 535
Number of words for Discussion: 748

Abstract

Perisomatic region of principal neurons in the cortical regions is innervated by three types of GABAergic interneurons, including parvalbumin-containing basket cells (PVBCs) and axo-axonic cells (AACs), as well as cholecystokinin and type 1 cannabinoid receptor-expressing basket cells (CCK/CB1BCs). These perisomatic inhibitory cell types can also be found in the basal nucleus of the amygdala, however, their output properties are largely unknown. Here, we performed whole-cell recordings in morphologically identified interneurons in slices prepared from transgenic mice, in which the GABAergic cells could be selectively targeted. By investigating the passive and active membrane properties of interneurons located within the basal amygdala, we observed that the three interneuron types had distinct single-cell properties. For instance, the input resistance, spike rate, accommodation in discharge rate, or after-hyperpolarization width at the half maximal amplitude separated the three interneuron types. Furthermore, we performed paired recordings from interneurons and principal neurons to uncover the basic features of unitary inhibitory postsynaptic currents (uIPSCs). We found that, although there was no difference in the magnitude of responses measured in the principal neurons, the uIPSCs originated from the distinct interneuron types differed in the rise time, failure rate, latency and short-term dynamics. Moreover, the asynchronous transmitter release induced by a train of action potentials was typical for the output synapses of CCK/CB1BCs. Our results suggest that, although the three perisomatic inhibitory cell types give rise to uIPSCs with similar magnitude, their distinct spiking characteristics may help to accomplish specific function in amygdala operation.

Introduction

Perisomatic region is a unique membrane surface of neurons, where the spiking can be most effectively controlled by inhibitory inputs (Cobb *et al.*, 1995; Miles *et al.*, 1996; Freund & Katona, 2007). In cortical networks three distinct types of GABAergic cells give rise to the innervation of the perisomatic region of principal cells (Somogyi *et al.*, 1998; Freund & Katona, 2007; Kepecs & Fishell, 2014). This is in contrast to other brain region, e.g. to the striatum or cerebellum, where only a single cell type is specialized to target the perisomatic domain of principal neurons (Pouzat & Hestrin, 1997; Koos & Tepper, 1999). Previous studies obtained in the neocortex and hippocampus have revealed that parvalbumin (PV)-containing axo-axonic cells (AACs) target specifically the axon initial segment of the principal cells (Somogyi, 1977; Katsumaru *et al.*, 1988; DeFelipe *et al.*, 1989), while two types of basket cells (BCs) expressing PV or a neuropeptide cholecytokinin (CCK) together with type 1 cannabinoid receptors (CB1) innervate the soma and the proximal dendrites of neurons (Freund *et al.*, 1986; Katsumaru *et al.*, 1988; Acsády *et al.*, 1996). Although these two BC types may terminate on the similar membrane surface of postsynaptic cells, they are distinct in many respects, including the spiking properties or firing activities during various brain states (Klausberger *et al.*, 2005; Somogyi & Klausberger, 2005). These results suggest that the role of these interneurons in circuit operation might be quite different (Freund, 2003).

The basal nucleus of the amygdala (BA) has been shown to play a critical role in several higher order cognitive operations, including the adequate responses to environmental challenges (LeDoux, 2000; Fanselow & Gale, 2003; Pape & Pare, 2010; Tovote *et al.*, 2015). Accumulating evidence suggests that, although layers cannot be distinguished in the BA, its microcircuit organization, such as the present of different cell types and their connectivity is similar to that observed in the neocortex or hippocampus (McDonald, 1992; Sah *et al.*, 2003). This notion is supported also by the facts that the perisomatic region of principal neurons in the BA is predominantly targeted by three types of GABAergic cells. AACs containing parvalbumin synapse specifically on the axon initial segment of amygdalar principal cells (Bienvenu *et al.*, 2012; Veres *et al.*, 2014), while PVBCs and CCK/CB1BCs have been shown to target the soma and the dendrites (Katona *et al.*, 2001; McDonald *et al.*, 2002; Muller *et al.*, 2006; Bienvenu *et al.*, 2012; Vereczki *et al.*, 2016). Thus, these interneurons are in a position to successfully regulate the output of the cortical parts of the amygdala. However, both the single-cell characteristics of the three perisomatic inhibitory cell types and the properties of their output synapses are largely unknown, which knowledge is necessary to understand the role they may fulfill in amygdalar function.

Here, we obtained *in vitro* whole-cell recordings from morphologically identified interneurons and characterized their passive and active membrane properties. To uncover the quality of the output synapses of the interneurons, paired recordings were performed. We found that three distinct types of GABAergic cells differed both in single-cell features and some of the characteristics of their output synapses, which may be critical to complete their diverse and complex function in network operation within the BA.

Materials and Methods

Experimental animals and slice preparation

All experiments were approved by the Committee of the Scientific Ethics of Animal Research (22.1/4027/003/2009) and were performed according to institutional guidelines of ethical code and the Hungarian Act of Animal Care and Experimentation (1998. XXVIII. Section 243/1998). Transgenic mice expressing either enhanced green fluorescent protein (eGFP) controlled by PV promoter (BAC-PV-eGFP, (Meyer *et al.*, 2002)) or red fluorescent protein under the control of CCK promoter were used (BAC-CCK-DsRed, (Mate *et al.*, 2013)) for interneuron labeling. Mice (postnatal days 20–30) were decapitated under deep isoflurane anaesthesia, and their brains were removed into ice cold cutting solution (in mM): 252 sucrose, 2.5 KCl, 26 $NaHCO_3$, 1 $CaCl_2$, 5 $MgCl_2$, 1.25 NaH_2PO_4, 10 glucose, bubbled with 95% O_2 / 5% CO_2 (carbogen gas). Horizontal slices of 200 µm thickness containing the amygdala region were prepared with a Leica VT1000S or VT1200S Vibratome (Wetzlar, Germany), and kept in an interface-type holding chamber containing artificial cerebrospinal fluid (ACSF) at 36 ºC that gradually cooled down to room temperature. ACSF contained (in mM) 126 NaCl, 2.5 KCl, 1.25 NaH_2PO4, 2 $MgCl_2$, 2 $CaCl_2$, 26 $NaHCO_3$, and 10 glucose saturated with 95% O_2–5% CO_2.

Electrophysiological recordings and analysis

After incubation, slices were transferred individually into a submerged type of recording chambers superfused with ACSF at 32±2 ºC with a flow rate of 2-3 ml/min. Whole-cell patch-clamp recordings were performed under visual guidance using differential interference contrast microscopy (Olympus BX61W). Fluorescent protein in neurons was excited by a mercury lamp or by a monochromator (Polychrome V, Till Photonics GmbH), and the fluorescence was visualized by a CCD camera (Hamamatsu Photonics, Japan). Patch pipettes were pulled from borosilicate glass capillaries with inner filament (Hilgenberg, Germany) using a DMZ-Universal Puller (Zeitz-Instrumente GmbH, Germany). Pipettes with 0.188 mm wall thickness were used and had a resistance of around 3-5 MΩ. Recordings in interneurons were obtained using K-gluconate-based intrapipette solution with a composition of (in mM): 110 K-gluconate, 4 NaCl, 2 Mg-ATP, 20 HEPES, 0,1 EGTA, 0.3 GTP (sodium salt), 10 phosphocreatine and 0.2% biocytin, adjusted to pH 7.3 using KOH and with an osmolarity of 290 mOsm/L. Electrical signals were detected with a Multiclamp 700B amplifier (Molecular Devices, Foster City, CA, USA), low-pass filtered at 2 kHz, digitized at 5 or 10 kHz with a PNI-6024E or a PNI-6040E board (National Instruments), and recorded with in-house data acquisition and stimulus software (Stimulog, courtesy of Prof. Zoltán Nusser, Institute of Experimental Medicine, Hungarian Academy of Sciences, Budapest, Hungary). Recordings were not corrected for junction potential.

After obtaining the whole-cell configuration in interneurons, we tested their voltage responses to a series of hyperpolarizing and depolarizing square current pulses of 800 ms duration and amplitudes between -100 and 100 pA at 10 pA step intervals, then up to 300 pA at 50 pA step intervals and finally up to 600 pA at 100 pA step intervals from a holding potential of -65 mV in each cell. Using voltage responses to the hyperpolarizing current injections, we calculated the input resistance, membrane capacitance, membrane time constant, and the relative sag amplitude with a custom-made program written in MATLAB (Zemankovics *et al.*, 2010). The action potential features and the firing characteristics were calculated from the voltage responses to the depolarizing current steps with an in-house analysis software SPIN 1.0.1 (courtesy of Prof. Zoltán Nusser)(Papp *et al.*, 2013). Accommodation index was calculated as the ratio of the values for the last and the first inter-spike intervals.

In paired recordings, the presynaptic cell was an interneuron identified by its fluorescent signal and the postsynaptic cell was a principal neuron (PN). The intrapipette solution used for the postsynaptic PN contained (in mM) 80 CsCl, 60 Cs-gluconate, 1 $MgCl_2$, 2 Mg-ATP, 3 NaCl, 10 HEPES, and 5 QX-314 (2(triethylamino)- *N*-(2,6-dimethylphenyl) acetamine), adjusted to pH 7.3 with CsOH, and the osmolarity was 295 mOsm/l. Presynaptic interneurons were held in current clamp mode near a membrane potential of -65 mV, and stimulated by brief current pulses (1.5 ms, 1-2 nA) to evoke action potentials. PNs were clamped at the holding potential of -65 mV. Series resistance (between 5-20 MΩ) was frequently monitored and compensated by 65%. Cells where the series resistance has changed more than 25% during recording were discarded from further analysis. The properties of postsynaptic responses were analyzed with EVAN 1.3 (courtesy of Professor Istvan Mody, Department of Neurology and Physiology, UCLA, CA) and Origin 8.6 (OriginLab Corp. Northampton, MA). The kinetic properties of unitary inhibitory postsynaptic currents (uIPSCs) were calculated with excluding the transmission failures. The latency of synaptic transmission was calculated by subtracting the time of the action potential peaks from the onset of the postsynaptic currents. This latter value was estimated by subtracting the rise time from the peak time of events calculated from the time of the action potential peaks. Calculation of asynchronous release was achieved by the comparison of the average charge (area under the curve) of all currents in a 100-ms-long time window before and after the action potential trains. To investigate the dynamics of the transmitter release, we calculated the average of uIPSC amplitudes in response to ten action potentials at different frequencies evoked in the presynaptic cell. These trains of action potentials were evoked at 0.05 Hz during each recording.

Post hoc anatomical identification of interneurons.

After recordings, the slices were fixed in 4 % PFA in 0.1 M PB (pH 7.4) overnight, followed by washout with 0.1 M PB several times. Biocytin-filled cells from PV-eGFP mice were visualized with Alexa 488-conjugated streptavidin (1:3000, Invitrogen), while filled interneurons recorded in slices prepared from CCK-DsRed mice were visualized with Cy3-conjugated streptavidin (1:1000; Sigma-Aldrich). If the visualization of biocytin in the axon collaterals of filled neurons was successful, then slices were embedded in agar (1%) and re-sectioned to 40 μm thickness. In each case, when interneurons were recorded in slices prepared from PV-eGFP mice, we separated axo-axonic cells from basket cells using double immunofluorescent staining for biocytin and rabbit anti-ankyrin G to visualize the biocytin-filled axon collaterals together with the axon initial segments (AIS) of neurons. When boutons of a labeled interneuron formed often close appositions with ankyrin G-immunostained profiles, the cell was identified as an axo-axonic cell (see for details, (Gulyas *et al.*, 2010; Veres *et al.*, 2014)). In case of CCK/CB_1BC cells, the CB1 positivity was tested (1:2000, Cayman)(Vereczki *et al.*, 2016). For illustration purposes, one interneuron from each group was used for reconstruction. In this case, biocytin was visualized using avidin-biotinylated horseradish peroxidase complex reaction (ABC; Vector Laboratories, Burlingame, CA, USA) with nickel-intensified 3,3-diaminobenzidine as a chromogen. After dehydration and embedding in Durcupan (Fluka), neurons with the most completed axonal and dendritic arborizations were selected for reconstruction with the aid of a drawing tube using a 40× or 100x objective.

For electron microscopy some sections from three filled PVBC and four filled AAC was processed where biocytin was visualized as above. The sections were then treated in 1% OsO_4, followed by 1% uranyl acetate, dehydrated in a graded series of ethanol, and embedded in epoxy resin (Durcupan; Fluka). Ultrathin sections of 60 nm thickness were cut for electron microscopic analysis, and the postsynaptic targets of 5–10 boutons of each examined cells

were identified. The remaining sections were processed for fluorescent double immunolabeling. They were treated with 0.2 mg ⁄ mL pepsin (Cat. No.: S3002; Dako) in 0.2 m HCl at 37_C for 5 min and were washed in 0.1 m PB similar to the procedure developed by Watanabe et al. (Watanabe *et al.*, 1998). Sections were treated with normal goat serum (NGS; 10%) made up in Tris-buffered saline (TBS, pH = 7.4) followed by incubation in mouse anti-Ankyrin G (1: 100; Santa Cruz Biotechnology) diluted in TBS containing 2% NGS and 0.3% Triton X-100. Following several washes in TBS, Cy3-conjugated goat anti-mouse (1:500; Jackson) was used to visualize the immunoreaction, while Alexa488-conjugated streptavidin (1:500; Invitrogen) to visualize the biocytin. Sections were then mounted on slides in Vectashield (Vector Laboratories). Images were taken using an AxioImager Z1 axioscope (Carl Zeiss MicroImaging GmbH, Germany) or Nikon C2 confocal microscope (CFI Plan Apo VC60X Oil objective, N.A. 1.40; z step size: 0.13 μm, xy: 0.08 μm/pixel).

Statistical analysis

For comparison of data with a non-normal distribution according to the Shapiro-Wilk test, the Mann-Whitney U test, Wilcoxon Signed Rank test and Kruskal-Wallis ANOVA (K-W ANOVA) was used. For the comparison of distributions, the two sample Kolmogorov-Smirnov test was used (K-S test). All statistics were performed using Origin 8.6 (Northampton, MA). Data are presented as mean ± SD unless indicated.

Results

Identification of different types of interneurons

All the recorded interneurons were tested for firing characteristics and filled with biocytin to allow *post hoc* visualization of their morphology (Fig. 1A). To distinguish AACs from other PV–containing interneurons, after recordings double immunofluorescent staining was performed to visualize the biocytin-filled axon collaterals together with the AISs, revealed with immunostaining against Ankyrin G (AnkG). PV cells forming close apposition with the AnkG-labeled segments were identified as AACs (n=29) at light microscopic level (Fig. 1D). Electron microscopic investigation showing symmetrical synaptic contact between boutons of this cell type and AIS confirmed this identification (Fig. 1E), in agreement with our recent study (Vereczki *et al.*, 2016). The PV-GFP cells targeting to postsynaptic segments other than AISs were grouped and named as PVBCs (Fig. 1B and C, n=34). From CCK interneuron population, only those neurons identified as CCK/CB1BCs, which were found to express CB1 (Fig. 1F, n=22).

Passive and active membrane characteristics of the perisomatic region-targeting interneurons in the BA

In the first part of this study, we compared the voltage responses of the three interneuron types upon injection of gradually-increasing depolarizing and hyperpolarizing current steps using whole-cell patch-clamp technique (Fig. 2A). Analysis revealed some marked differences among the cell types. Overall, both the passive and active membrane properties of PVBCs and AACs were more similar than those characterized CCK/CB1BCs. Namely, PVBCs and AACs had narrow action potentials and a fast-spiking character with modest accommodation in firing (Table 1). In contrast, CCK/CB1BCs had wider action potentials and a regular spiking character showing a profound accommodation in spiking (Table 1). Notably,

although the membrane capacitance between PVBCs and AACs differed, their membrane time constants were similar (Fig. 2D), offset by input resistance (Table 1). The membrane time constant for CCK/CB1BCs, however, was significantly slower compared to those obtained for PV-expressing cells (Fig. 2D). Interestingly, the width of the after-hyperpolarization measured at the half maximum amplitude, but not at other values differentiated the three cell types (Fig. 2E, Table 1).

In addition, we performed a detailed analysis of interneuron spiking. First, we obtained the input-output relationship for firing by plotting the spiking frequency as a function of the intracellularly-injected current step magnitude (Fig. 2B, C). We found that at low current magnitudes interneurons had similar response curves, which deviated significantly upon larger current injections. At a given current input, AACs displayed the highest firing rate, while CCK/CB1BCs the lowest (Fig. 2C). In accord, the difference in the maximum firing rate evoked upon the largest depolarization among the three interneuron types was significant (Table 1). Second, we compared the inter-spike intervals between the first two and the last two action potentials. Interestingly, the inter-spike intervals for the first and for the last two spikes were significantly shorter recorded in AACs than those in BCs (Fig. 2D, Table 1).

These data show that, while the single-cell electrophysiological properties of PV-containing interneurons are rather similar, several of these features are markedly distinct of those obtained in CCK/CB1BCs.

Properties of synaptic communication between perisomatic region-targeting interneurons and PNs in the BA

In addition to the spiking capability of examined interneuron types, these GABAergic cells might also differ in the features at their output synapses, which could profoundly impact the function they play in the local microcircuits. To directly address this question we obtained paired recordings between presynaptic interneurons and postsynaptic PNs. By evoking unitary inhibitory postsynaptic currents (uIPSCs) in PNs by single action potentials in presynaptic GABAergic cells, we determined the basic properties of synaptic transmission at these contacts, including the peak amplitude (including failures), potency (excluding failures), 10-90% rise time and decay time constant, the synaptic latency of transmission (i.e. the time between the peak of action potentials and the beginning of the uIPSC) and the probability of transmission failures. Statistical comparisons of these parameters revealed that the output synapses of CCK/CB1BCs had slower 10-90% rise time and longer synaptic latency compared to those observed in PV-containing cell-PN pairs (Fig. 3, Table 2). In addition, the probability of transmission failures at CCK/CB1BCs output synapses was different in comparison with the AAC output synapses (Fig. 3, Table 2). These results show that the overall physiological properties of synaptic contacts tested by single action potentials are rather similar among interneurons innervating the perisomatic region.

Next, we compared the short-term dynamics at these synapses by evoking 10 action potentials at different frequencies (Fig. 4). In general, we found that depending on the spiking frequency of presynaptic neurons the postsynaptic responses in PNs showed depression (Fig. 4B). Larger the spiking frequency is, larger depression in the magnitude of postsynaptic events could be observed. To quantify these differences we compared the second ($IPSC_2$) and the tenth ($IPSC_{10}$) peak amplitude of evoked uIPSCs to the first ($IPSC_1$) at different frequencies. The output synapses of PVBCs displayed profound depression in $IPSC_2/IPSC_1$ ratios above 5 Hz, whereas there was no change in the magnitude at output synapses of other cell types (Fig. 4*C*). In contrast, the $IPSC_{10}/IPSC_1$ ratios of unitary events for each cell type showed marked depression to a similar extent (Fig. 4C). These data indicate that while

synaptic properties of perisomatic contacts evoked by single action potentials are rather similar, these connections might differ in their short-term plasticity. Specifically, when presynaptic PVBCs, but not AACs or CCK/CB_1BCs fire doublets of spikes, depression in responses already could be detected. However, higher number of spikes at the output synapses of all perisomatic region-targeting interneuron types evokes a marked depression in uIPSC amplitudes recorded in postsynaptic PNs.

Finally, we asked whether, in addition to the transmitter release synchronized to action potentials, asynchronous release of neurotransmitter molecules followed by a train of action potentials could be detected at the output synapses of these interneuron types. To this end, we measured the charge following the action potential trains evoked at different frequencies (see Methods for details). We found that at synaptic contacts originated from CCK/CB1BCs, prolonged synaptic inhibition followed the action potential train, as a sign for asynchronous GABA release, was substantial, which magnitude was frequency-dependent (Fig. 5). Much smaller charge following the action potentials could be registered at the output synapses of PVBCs, while no asynchronous transmitter release was found at the connections formed by AACs (Fig. 5B, C). These results show that the perisomatic inhibition from CCK/CB1BCs, but not from PV-expressing interneurons could be significantly prolonged after the trains of action potentials at higher frequencies.

Discussion

Our main findings are as follows: The three interneuron types substantially differ in (1) single-cell features, including the input resistance, spike rate, accommodation in discharge rate, or after-hyperpolarization width at the half maximal amplitude separated the three interneuron types; (2) in the properties of their output synapses, such as the rise time, failure rate, latency and (3) in the short-term dynamics of multiple events and (4) the amount of asynchronously released GABA after a train of action potentials.

The use of transgenic mouse lines allowed us to selectively target different interneuron types in slice preparations and perform single-cell and paired recordings. In accord with previous findings obtained in the amygdala (Washburn & Moises, 1992; Rainnie *et al.*, 1993; Rainnie *et al.*, 2006; Woodruff & Sah, 2007), our results indicated that PV-expressing interneurons had a fast spiking character, narrow spike width, fast after-hyperpolarization, fast membrane time constant, while CCK/CB_1BCs showed accommodation in firing, wider action potentials, slower after-hyperpolarization and membrane time constant (Jasnow *et al.*, 2009). These data are in full agreement with those found in other cortical areas (Galarreta & Hestrin, 1999; Glickfeld & Scanziani, 2006; Galarreta *et al.*, 2008; Daw *et al.*, 2009; Szabo *et al.*, 2010; Cea-del Rio *et al.*, 2011). By comparing the single-cell features of PVBCs and AACs, we found that their properties were similarly distinct as it has been observed in the hippocampus or neocortex (Papp *et al.*, 2013; Povysheva *et al.*, 2013). Both PV-expressing cell types can discharge at high firing rate *in vitro* and *in vivo* (Klausberger *et al.*, 2003; Bienvenu *et al.*, 2012; Massi *et al.*, 2012), and, notably, they often fire doublets of action potentials *in vivo* (Viney *et al.*, 2013; Varga *et al.*, 2014). Similar to the noxious stimulus-driven responses observed *in vivo* (Bienvenu *et al.*, 2012), we showed here that AACs cells display higher firing frequency activation to the same current steps. By analyzing the inter-spike intervals between the first two action potentials evoked by the largest depolarizing step, we found that AACs could discharge spikes at 300-350 Hz, while the PVBCs (and CCK/CB_1BCs) did not spike with higher frequency than 200 Hz. This particular characteristic in spiking of fast spiking interneurons might be a valuable biomarker for distinguishing these two interneuron types displaying the narrowest spikes in intact animals, if one analyses the inter-spike intervals of double spikes during distinct brain states.

The features of the output synapses of perisomatic region-targeting interneurons, however, was previously only studied for PV-expressing cells without separation of PVBCs and AACs (Woodruff & Sah, 2007). Therefore, our study is the first to provide detailed comparative analysis of the synaptic properties of the three interneuron types innervating the perisomatic region of PNs. As we found in the hippocampus (Szabo *et al.*, 2010), these cell types gave rise to synaptic currents with fast rise time indicating the perisomatic origin of the postsynaptic events recorded in the PNs. Importantly, the short-term dynamics at the output synapses of the three interneurons were different and showed frequency dependence, implying that at a given activity pattern the three interneurons could provide specific GABAergic input onto the soma-near region of PNs (Klausberger & Somogyi, 2008; Varga *et al.*, 2014). These differences in synaptic dynamics might be important in the temporal control of spiking activities of PNs. Finally, the observed asynchronous release at the output synapses of CCK/CB_1BCs is likely to be a specific feature of these interneurons in cortical structures, because similar data have been obtained earlier in the hippocampus by several groups (Hefft & Jonas, 2005; Daw *et al.*, 2009; Szabo *et al.*, 2010). Previous studies showed that Ca^{2+} enters the terminals of PVBCs via P/Q-type voltage-gated Ca^{2+} channels that are in the active zone of presynaptic terminals which allows the axon endings of PVBCs (and probably of AACs as well) to release GABA upon action potential discharge with high probability and with precise timing (Bucurenciu *et al.*, 2008). In contrast, the axon terminals of RSBCs are equipped with N-type voltage-gated Ca^{2+} channels that are probably located at a distance from active zone (Wilson *et al.*, 2001; Hefft & Jonas, 2005), which could cause longer delay in the time of transmitter release and prolongs the transmitter release upon firing at high frequencies.

These results collectively suggest that the three main interneuron types innervating the perisomatic region of PNs may be differentially embedded into the local amygdalar circuits and having distinct physiological characteristics, therefore they can fulfill specific function(s) in circuit operation during various brain states.

Acknowledgements

This work is supported by a fellowship of the Hungarian Academy of Sciences awarded to NH (Lendület, LP2012-23) and the National Office for Research and Technology (OMFB-01678/2009). We thank Profs Hannah Monyer and Gábor Szabó for providing BAC-PV-eGFP mice and BAC-CCK-DsRed mice, respectively, Noémi Holderith for providing some data. The authors are grateful to Erzsébet Gregori and Éva Krizsán for their excellent technical assistance. We also thank László Barna, the Nikon Microscopy Center at the Institute of Experimental Medicine, Nikon Austria GmbH, and Auro-Science Consulting, Ltd., for kindly providing microscopy support. The authors declare no competing financial interests.

Figure legends

Figure 1. Morphological properties and anatomical identification of parvalbumin-containing basket cells (PVBC) and axo-axonic cells (AAC) as well as cholecystokinin/cannabinoid receptor type 1-expressing basket cells (CCK/CB1BC) in the basolateral complex of the mouse amygdala. (**A**) Camera lucida reconstructions and the localization of representative biocytin-labeled neurons in horizontal slices prepared from the mouse amygdala region. Soma and dendrites are shown in black and axonal arbor in orange (PVBC), green (AAC) or red (CCK/CB1BC). (**B**) Double immunofluorescent labeling shows that biocytin-filled axon terminals (b) of a PVBC cell (green; arrowheads) avoid Ankyrin G-labeled axon initial segments (AIS) (red; arrows). (**C**) A bouton (b) of the same PVBC forms a symmetrical synapse (marked by an arrow in the inset) on the soma (s) of a postsynaptic cell. (**D**) Double immunofluorescent labeling as in **C** shows tight appositions of boutons belonging to a biocytin-filled PV-GFP neuron with AISs, identifying this cell type as AAC. (**E**) An electron micrograph shows a biocytin-labeled axon terminal (b) of an AAC forming a symmetrical synapse (arrow; inset) on an AIS. **(F)** Confocal images indicate that biocytin-filled axon terminals of a CCK/DsRed cell (arrowheads, in red) co-express CB1 receptor (green).

Figure 2. Distinct single-cell electrophysiological properties of three interneuron types targeting the perisomatic region of the principal neurons in the BA. (**A**) Voltage responses to depolarizing (400 pA) and hyperpolarizing current steps (from -10 to -100 pA in increments of 10 pA). (**B**) Voltage responses to depolarizing current steps (150, 250, and 400 pA) injected around a holding potential of -65 mV. (**C**) Average frequency-input current relationships of the three interneuron types measured at a membrane potential of -65 mV. Data are presented as mean ± SEM. Significant difference was found between the three groups (a), between PVBC and CCK/CB1BC, and between AAC and CCK/CB1BC (b), between AAC and CCK/CB1BC (c), and between PVBC and AAC (d). (at 100 pA: ANOVA $p=0.041$, AAC vs. PVBC: $p=0.043$; at 200 pA: ANOVA $p=0.01$, AAC vs. CCK/CB1BC: $p=0.003$; at 250 pA: ANOVA $p<0.001$, PVBC vs. AAC: $p=0.037$, PVBC vs. CCK/CB1BC: $p=0.046$, AAC vs. CCK/CB1BC: $p<0.001$; at 300 pA: ANOVA $p<0.001$, PVBC vs. AAC: $p=0.049$; PVBC vs. CCK/CB1BC: $p=0.027$; AAC vs. CCK/CB1BC: $p<0.001$; at 400 pA: ANOVA $p<0.001$, PVBC vs. AAC: $p=0.037$; PVBC vs. CCK/CB1BC: $p<0.001$; AAC vs. CCK/CB1BC: $p<0.001$; at 500pA: ANOVA $p<0.001$, PVBC vs. CCK/CB1BC: $p<0.001$; AAC vs. CCK/CB1BC: $p=0.004$). (**D**) Single-cell properties are distinct in the three cell types. Here on the graphs and in Fig. 3 each line represents a value from an individual cell. Bars show the median values in each group and asterisks indicate significant differences. Comparison for membrane time constant ($p<0.001$, ANOVA), after-hyperpolarization half-width (AHP 50%, $p<0.001$, ANOVA) and inter-spike interval (ISI) for the first two spike at maximal firing rate ($p<0.001$, ANOVA) are shown. Significance levels are * $p<0.05$. For more details, see **Table 1**.

Figure 3. Basic properties of synaptic transmission in perisomatic region-targeting interneuron-PN pairs. (**A**) Examples obtained in paired recordings, where single action potentials were evoked in the three distinct types of interneurons (bottom traces), and the postsynaptic currents were recorded in the PNs (top traces). Ten consecutive traces are superimposed (gray) with the average of all traces (black). (**B**) Comparison of the peak amplitude, the synaptic potency, 10-90% rise time, the probability of failures, the decay time constant, and the latency measured at unitary connections between interneurons and PNs. Asterisks indicate significant differences, * $p<0.05$. For more details, see **Table 2**.

Figure 4. Short-term dynamics of transmitter release at the output synapses of the three perisomatic region-targeting interneurons. (**A**) Representative average IPSCs (bottom traces) in response to ten action potentials at a frequency of 30 Hz (upper traces). (**B**) Summary of the release dynamics evaluated at 30 Hz in PVBC- (n=10), AAC- (n=12) and CCK/CB1BC-PN pairs (n=7). Amplitude values in each case were normalized to the first peak. Tau values were obtained by exponential fit to data points in summary plots, showing distinct dynamical properties at 30 Hz. (**C**) Frequency-dependent changes in short-term plasticity. Ratios of $IPSC_2/IPSC_1$ and $IPSC_{10}/IPSC_1$ calculated at distinct frequencies indicate the different properties in release at the unitary connections giving rise by the three interneuron types. Data are presented as mean ± SEM. * $p<0.05$.

Figure 5. Asynchronous transmitter release at the output synapses of the three perisomatic region-targeting interneurons. (**A**) Representative postsynaptic events in response to ten action potentials (upper traces) evoked at 30 Hz. Averaged traces in black are superimposed on ten consecutive events shown in grey. The magnified 100-ms-long periods before and after the action potential trains used to estimate the amount of asynchronous transmitter release are shown. In CCK/CB1BC-PN pairs, the charge following the action potential train is clearly larger than before. (**B**) Summary of the frequency-dependent asynchronous release in the three types of interneuron-PN pairs. A robust increase in release was characteristics at the output synapses of CCK/CB1BCs at 20 Hz or higher frequencies. (**C**) Comparison of the magnitude of asynchronous release in the three interneuron-PN pairs evoked by 30 Hz. * $p<0.05$, *** $p<0.001$.

Table 1. Single-cell properties of the three perisomatic region-targeting interneuron types in the BA. Data are presented as the median with the first and third quartiles in parentheses. Significant differences shown in bold were determined by Kruskal-Wallis ANOVA and Mann-Whitney (MW) U test.

Parameters	**AAC (n=18-19)**	**PVBC (n=22-26)**	**CCK/CB1 BC (n=14)**	**Kruskal-Wallis ANOVA**	**AAC-PVBC MW test**	**AAC-CCK/CB1BC MW test**	**PVBC-CCK/CB1BC MW test**
Rheobase (pA)	150 (100, 150)	300 (150, 400)	90 (70, 150)	**<0.001**	<0.001	0.049	<0.001
AP threshold (mV)	-38.1 (-39.7, -36.9)	-37.2 (-40.7, -33.6)	-41 (-43.9, -37.5)	0.06387	n/a	n/a	n/a
AP amplitude (mV)	63.7 (58.1, 75.5)	55.85 (49.9, 64.2)	73.65 (62.3, 78.6)	**0.003**	0.039	0.13	0.001
AP half-width (ms)	0.3 (0.3, 0.4)	0.3 (0.3, 0.4)	0.7 (0.6, 0.8)	**<0.001**	0.15	<0.001	<0.001
Spike rate (Hz)	177.5 (157.5, 193.8)	110 (92.5, 138.75)	30 (27, 40)	**<0.001**	<0.001	<0.001	<0.001
Accommoda-tion ratio	2 (1.89, 2.23)	1.445 (1.29, 1.65)	4.755 (4.07, 5.69)	**<0.001**	<0.001	<0.001	<0.001
Input resistance (MOhm)	113.45 (109.3, 120.8)	77.15 (62.28, 107.9)	160.3 (130.3, 200.6)	**<0.001**	0.002	<0.001	<0.001
AHP amplitude (mV)	16.9 (16.2, 19.7)	21 (18.9, 23.4)	17.9 (15.4, 19.4)	**0.0031**	0.004	1	0.005
AHP 25% decay (ms)	9.1 (4.8, 21.8)	9.9 (6.7, 15.9)	45.6 (33.3, 58.4)	**<0.001**	0.82	<0.001	<0.001
AHP 50% decay (ms)	27.3 (18.9, 35)	17.4 (14.6, 28.1)	76.95 (60.2, 119.9)	**<0.001**	0.036	<0.001	<0.001
AHP 75% decay (ms)	33.9 (26.1, 43.1)	26.9 (21.2, 37.7)	113.85 (87.9, 156.6)	**<0.001**	0.16	<0.001	<0.001
Ratio of AP amplitude adaptation	0.7 (0.62, 0.75)	0.8 (0.68, 0.88)	0.83 (0.75, 0.91)	**0.003**	0.011	0.001	0.48
Membrane time constant (ms)	12.63 (10.56, 13.6)	9.53 (8.26, 12.1)	16.9 (13.48, 18.18)	**<0.001**	0.057	0.001	<0.001
Membrane capacitance (pF)	100.82 (84.56, 120.7)	137.95 (93.62, 174.7)	104.6 (92.41, 110.2)	**0.04**	0.035	0.81	0.033
Relative sag amplitude	0.123 (0.096, 0.168)	0.1 (0.068, 0.14)	0.196 (0.112, 0.235)	**0.035**	0.19	0.06	0.024
ISI between the first two spikes	3 (2.8, 3.4)	6.1 (5, 9)	6 (5.7, 7.4)	**<0.001**	<0.001	<0.001	0.91
ISI between the last two spikes	6.2 (5.4, 7.4)	10.7 (8.2, 11.8)	33.6 (23.6, 38.2)	**<0.001**	<0.001	<0.001	<0.001

AP, action potential; AHP, after hyperpolarization, ISI, inter-spike interval.

Table 2. Summary of uIPSC properties. Data are presented as the median with the first and third quartiles in parentheses. P values represent the results of the statistical comparison of *PVBC vs. AAC, # AAC vs. CCK/CB1BC and +CCK/CB1BC vs. PVBC using the Mann-Whitney U test after Kruskal-Wallis ANOVA.

	PVBC			**AAC**			**CCK/CB1BC**		
Parameter	Median	*p*-value*	n	Median	*p*-value#	n	Median	*p*-value+	n
Peak amplitude (pA)	339.4 (156.5-605.7)	0.056	8	310.3 (265.0-400.0)	0.056	10	152.6 (97.7-232.5)	0.056	8
Potency (pA)	340.0 (160.5-605.7)	0.094	8	310.3 (265.0-400.0)	0.094	10	177.6 (109.9-234.7)	0.094	8
Rise time (10-90%, ms)	0.63 (0.47-0.66)	0.450	8	0.50 (0.45-0.57)	**0.001**	10	1.05 (0.93-1.27)	**0.004**	8
Decay time constant (ms)	6.31 (5.30-7.48)	0.115	7	6.91 (6.52-8.21)	0.115	10	8.49 (6.77-9.45)	0.115	8
Probability of failure	0 (0-0.05)	0.180	8	0 (0-0)	**0.002**	10	0.04 (0.02-0.021)	0.067	8
Latency (ms)	0.92 (0.78-1.01)	**0.003**	8	1.33 (1.09-1.64)	0.965	10	1.42 (1.06-2.04)	**0.018**	8

Acsády, L., Gorcs, T.J. & Freund, T.F. (1996) Different populations of vasoactive intestinal polypeptide- immunoreactive interneurons are specialized to control pyramidal cells or interneurons in the hippocampus. *Neuroscience*, **73**, 317-334.

Bienvenu, T.C., Busti, D., Magill, P.J., Ferraguti, F. & Capogna, M. (2012) Cell-type-specific recruitment of amygdala interneurons to hippocampal theta rhythm and noxious stimuli in vivo. *Neuron*, **74**, 1059-1074.

Bucurenciu, I., Kulik, A., Schwaller, B., Frotscher, M. & Jonas, P. (2008) Nanodomain coupling between Ca2+ channels and Ca2+ sensors promotes fast and efficient transmitter release at a cortical GABAergic synapse. *Neuron*, **57**, 536-545.

Cea-del Rio, C.A., Lawrence, J.J., Erdelyi, F., Szabo, G. & McBain, C.J. (2011) Cholinergic modulation amplifies the intrinsic oscillatory properties of CA1 hippocampal cholecystokinin-positive interneurons. *J Physiol*, **589**, 609-627.

Cobb, S.R., Buhl, E.H., Halasy, K., Paulsen, O. & Somogyi, P. (1995) Synchronization of neuronal activity in hippocampus by individual GABAergic interneurons. *Nature*, **378**, 75-78.

Daw, M.I., Tricoire, L., Erdelyi, F., Szabo, G. & McBain, C.J. (2009) Asynchronous transmitter release from cholecystokinin-containing inhibitory interneurons is widespread and target-cell independent. *The Journal of neuroscience : the official journal of the Society for Neuroscience*, **29**, 11112-11122.

DeFelipe, J., Hendry, S.H.C. & Jones, E.G. (1989) Visualization of chandelier cell axons by parvalbumin immunoreactivity in monkey cerebral-cortex. *PNAS*, **86**, 2093-2097.

Fanselow, M.S. & Gale, G.D. (2003) The amygdala, fear, and memory. *Annals of the New York Academy of Sciences*, **985**, 125-134.

Freund, T.F. (2003) Interneuron Diversity series: Rhythm and mood in perisomatic inhibition. *Trends in neurosciences*, **26**, 489-495.

Freund, T.F. & Katona, I. (2007) Perisomatic inhibition. *Neuron*, **56**, 33-42.

Freund, T.F., Maglóczky, Z., Soltész, I. & Somogyi, P. (1986) Synaptic connections, axonal and dendritic patterns of neurons immunoreactive for cholecystokinin in the visual cortex of the cat. *Neuroscience*, **19**, 1133-1159.

Galarreta, M., Erdelyi, F., Szabo, G. & Hestrin, S. (2008) Cannabinoid sensitivity and synaptic properties of 2 GABAergic networks in the neocortex. *Cerebral cortex*, **18**, 2296-2305.

Galarreta, M. & Hestrin, S. (1999) A network of fast-spiking cells in the neocortex connected by electrical synapses. *Nature*, **402**, 72-75.

Glickfeld, L.L. & Scanziani, M. (2006) Distinct timing in the activity of cannabinoid-sensitive and cannabinoid-insensitive basket cells. *Nat Neurosci*, **9**, 807-815.

Gulyas, A.I., Szabo, G.G., Ulbert, I., Holderith, N., Monyer, H., Erdelyi, F., Szabo, G., Freund, T.F. & Hajos, N. (2010) Parvalbumin-containing fast-spiking basket cells generate the field potential oscillations induced by cholinergic receptor activation in the hippocampus. *J Neurosci*, **30**, 15134-15145.

Hefft, S. & Jonas, P. (2005) Asynchronous GABA release generates long-lasting inhibition at a hippocampal interneuron-principal neuron synapse. *Nat Neurosci*, **8**, 1319-1328.

Jasnow, A.M., Ressler, K.J., Hammack, S.E., Chhatwal, J.P. & Rainnie, D.G. (2009) Distinct subtypes of cholecystokinin (CCK)-containing interneurons of the basolateral amygdala identified using a CCK promoter-specific lentivirus. *J Neurophysiol*, **101**, 1494-1506.

Katona, I., Rancz, E.A., Acsady, L., Ledent, C., Mackie, K., Hajos, N. & Freund, T.F. (2001) Distribution of CB1 cannabinoid receptors in the amygdala and their role in the control of GABAergic transmission. *J Neurosci*, **21**, 9506-9518.

Katsumaru, H., Kosaka, T., Heizmann, C.W. & Hama, K. (1988) Immunocytochemical study of GABAergic neurons containing the calcium-binding protein parvalbumin in the rat hippocampus. *Exp.Brain Res.*, **72**, 347-362.

Kepecs, A. & Fishell, G. (2014) Interneuron cell types are fit to function. *Nature*, **505**, 318-326.

Klausberger, T., Magill, P.J., Marton, L.F., Roberts, J.D., Cobden, P.M., Buzsaki, G. & Somogyi, P. (2003) Brain-state- and cell-type-specific firing of hippocampal interneurons in vivo. *Nature*, **421**, 844-848.

Klausberger, T., Marton, L.F., O'Neill, J., Huck, J.H., Dalezios, Y., Fuentealba, P., Suen, W.Y., Papp, E., Kaneko, T., Watanabe, M., Csicsvari, J. & Somogyi, P. (2005) Complementary roles of cholecystokinin- and parvalbumin-expressing GABAergic neurons in hippocampal network oscillations. *The Journal of neuroscience : the official journal of the Society for Neuroscience*, **25**, 9782-9793.

Klausberger, T. & Somogyi, P. (2008) Neuronal diversity and temporal dynamics: the unity of hippocampal circuit operations. *Science*, **321**, 53-57.

Koos, T. & Tepper, J.M. (1999) Inhibitory control of neostriatal projection neurons by GABAergic interneurons. *Nat Neurosci*, **2**, 467-472.

LeDoux, J.E. (2000) Emotion circuits in the brain. *Annu Rev Neurosci*, **23**, 155-184.

Massi, L., Lagler, M., Hartwich, K., Borhegyi, Z., Somogyi, P. & Klausberger, T. (2012) Temporal dynamics of parvalbumin-expressing axo-axonic and basket cells in the rat medial prefrontal cortex in vivo. *J Neurosci*, **32**, 16496-16502.

Mate, Z., Poles, M.Z., Szabo, G., Bagyanszki, M., Talapka, P., Fekete, E. & Bodi, N. (2013) Spatiotemporal expression pattern of DsRedT3/CCK gene construct during postnatal development of myenteric plexus in transgenic mice. *Cell Tissue Res*, **352**, 199-206.

McDonald, A.J. (1992) Projection neurons of the basolateral amygdala: a correlative Golgi and retrograde tract tracing study. *Brain Res Bull*, **28**, 179-185.

McDonald, A.J., Muller, J.F. & Mascagni, F. (2002) GABAergic innervation of alpha type II calcium/calmodulin-dependent protein kinase immunoreactive pyramidal neurons in the rat basolateral amygdala. *The Journal of comparative neurology*, **446**, 199-218.

Meyer, A.H., Katona, I., Blatow, M., Rozov, A. & Monyer, H. (2002) In vivo labeling of parvalbumin-positive interneurons and analysis of electrical coupling in identified neurons. *J Neurosci*, **22**, 7055-7064.

Miles, R., Toth, K., Gulyás, A.I., Hajos, N. & Freund, T.F. (1996) Differences between somatic and dendritic inhibition in the hippocampus. *Neuron*, **16**, 815-823.

Muller, J.F., Mascagni, F. & McDonald, A.J. (2006) Pyramidal cells of the rat basolateral amygdala: synaptology and innervation by parvalbumin-immunoreactive interneurons. *The Journal of comparative neurology*, **494**, 635-650.

Pape, H.C. & Pare, D. (2010) Plastic synaptic networks of the amygdala for the acquisition, expression, and extinction of conditioned fear. *Physiological reviews*, **90**, 419-463.

Papp, O.I., Karlocai, M.R., Toth, I.E., Freund, T.F. & Hajos, N. (2013) Different input and output properties characterize parvalbumin-positive basket and Axo-axonic cells in the hippocampal CA3 subfield. *Hippocampus*, **23**, 903-918.

Pouzat, C. & Hestrin, S. (1997) Developmental regulation of basket/stellate cell-->Purkinje cell synapses in the cerebellum. *J Neurosci*, **17**, 9104-9112.

Povysheva, N.V., Zaitsev, A.V., Gonzalez-Burgos, G. & Lewis, D.A. (2013) Electrophysiological heterogeneity of fast-spiking interneurons: chandelier versus basket cells. *PloS one*, **8**, e70553.

Rainnie, D.G., Asprodini, E.K. & Shinnick-Gallagher, P. (1993) Intracellular recordings from morphologically identified neurons of the basolateral amygdala. *Journal of neurophysiology*, **69**, 1350-1362.

Rainnie, D.G., Mania, I., Mascagni, F. & McDonald, A.J. (2006) Physiological and morphological characterization of parvalbumin-containing interneurons of the rat basolateral amygdala. *The Journal of comparative neurology*, **498**, 142-161.

Sah, P., Faber, E.S., Lopez De Armentia, M. & Power, J. (2003) The amygdaloid complex: anatomy and physiology. *Physiological reviews*, **83**, 803-834.

Somogyi, P. (1977) A specific 'axo-axonal' interneuron in the visual cortex of the rat. *Brain Res.*, **136**, 345-350.

Somogyi, P. & Klausberger, T. (2005) Defined types of cortical interneurone structure space and spike timing in the hippocampus. *J Physiol*, **562**, 9-26.

Somogyi, P., Tamás, G., Lujan, R. & Buhl, E.H. (1998) Salient features of synaptic organisation in the cerebral cortex. *Brain Res Rev*, **26**, 113-135.

Szabo, G.G., Holderith, N., Gulyas, A.I., Freund, T.F. & Hajos, N. (2010) Distinct synaptic properties of perisomatic inhibitory cell types and their different modulation by cholinergic receptor activation in the CA3 region of the mouse hippocampus. *Eur J Neurosci*, **31**, 2234-2246.

Tovote, P., Fadok, J.P. & Luthi, A. (2015) Neuronal circuits for fear and anxiety. *Nat Rev Neurosci*, **16**, 317-331.

Varga, C., Oijala, M., Lish, J., Szabo, G.G., Bezaire, M., Marchionni, I., Golshani, P. & Soltesz, I. (2014) Functional fission of parvalbumin interneuron classes during fast network events. *Elife*, **3**.

Vereczki, V.K., Veres, J.M., Muller, K., Nagy, G.A., Racz, B., Barsy, B. & Hajos, N. (2016) Synaptic Organization of Perisomatic GABAergic Inputs onto the Principal Cells of the Mouse Basolateral Amygdala. *Frontiers in neuroanatomy*, **10**, 20.

Veres, J.M., Nagy, G.A., Vereczki, V.K., Andrasi, T. & Hajos, N. (2014) Strategically positioned inhibitory synapses of axo-axonic cells potently control principal neuron spiking in the basolateral amygdala. *The Journal of neuroscience : the official journal of the Society for Neuroscience*, **34**, 16194-16206.

Viney, T.J., Lasztoczi, B., Katona, L., Crump, M.G., Tukker, J.J., Klausberger, T. & Somogyi, P. (2013) Network state-dependent inhibition of identified hippocampal CA3 axo-axonic cells in vivo. *Nat Neurosci*, **16**, 1802-1811.

Washburn, M.S. & Moises, H.C. (1992) Electrophysiological and morphological properties of rat basolateral amygdaloid neurons in vitro. *J Neurosci*, **12**, 4066-4079.

Watanabe, M., Fukaya, M., Sakimura, K., Manabe, T., Mishina, M. & Inoue, Y. (1998) Selective scarcity of NMDA receptor channel subunits in the stratum lucidum (mossy fibre-recipient layer) of the mouse hippocampal CA3 subfield. *Eur J Neurosci*, **10**, 478-487.

Wilson, R.I., Kunos, G. & Nicoll, R.A. (2001) Presynaptic specificity of endocannabinoid signaling in the hippocampus. *Neuron*, **31**, 453-462.

Woodruff, A.R. & Sah, P. (2007) Networks of parvalbumin-positive interneurons in the basolateral amygdala. *The Journal of neuroscience : the official journal of the Society for Neuroscience*, **27**, 553-563.

Zemankovics, R., Kali, S., Paulsen, O., Freund, T.F. & Hajos, N. (2010) Differences in subthreshold resonance of hippocampal pyramidal cells and interneurons: the role of h-current and passive membrane characteristics. *J Physiol*, **588**, 2109-2132.

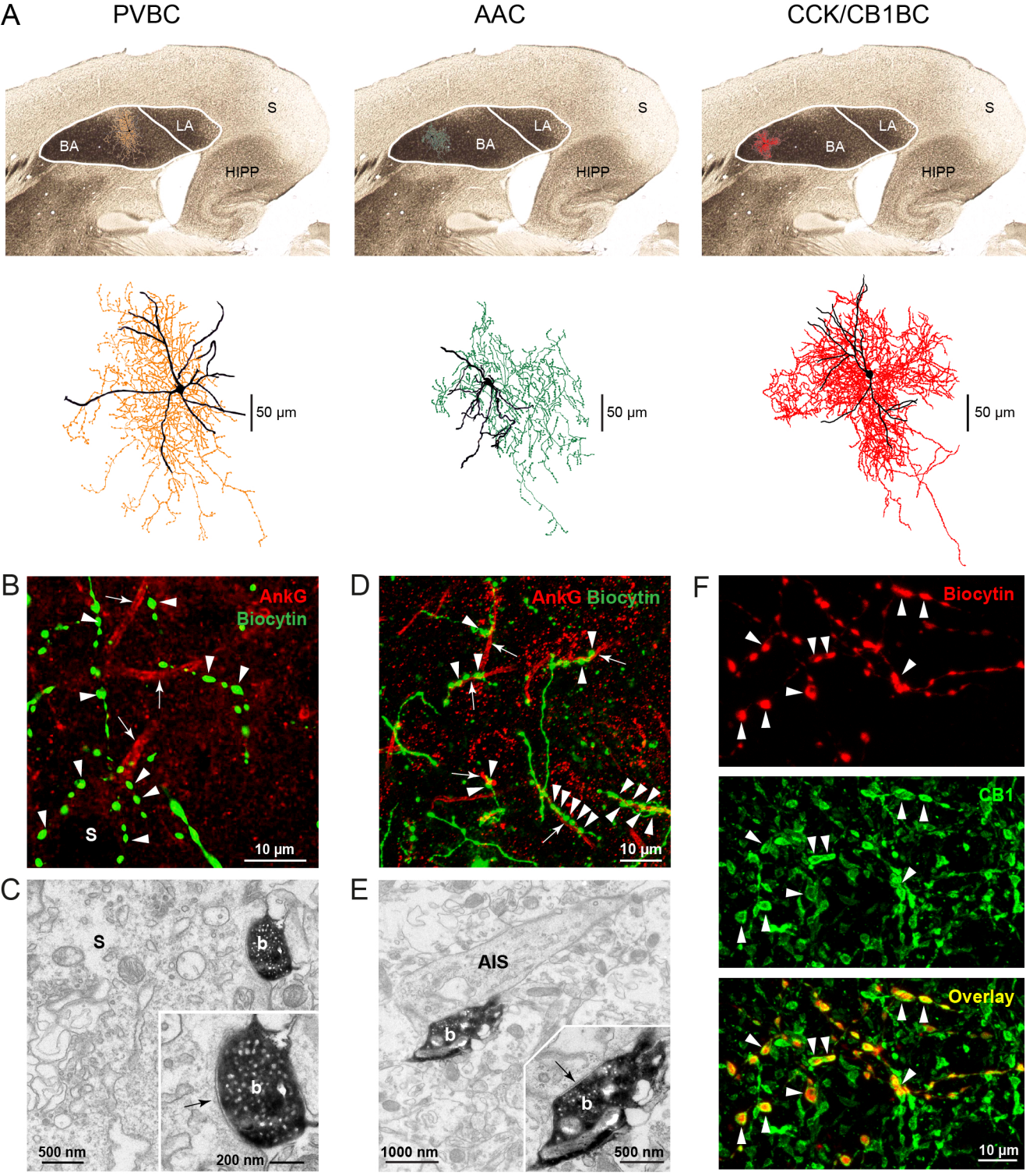
A
PVBC
AAC
CCK/CB1BC
BA
LA
S
HIPP
50 µm
B
AnkG
Biocytin
S
10 µm
D
AnkG Biocytin
10 µm
F
Biocytin
CB1
Overlay
10 µm
C
S
b
500 nm
200 nm
E
AIS
b
1000 nm
500 nm

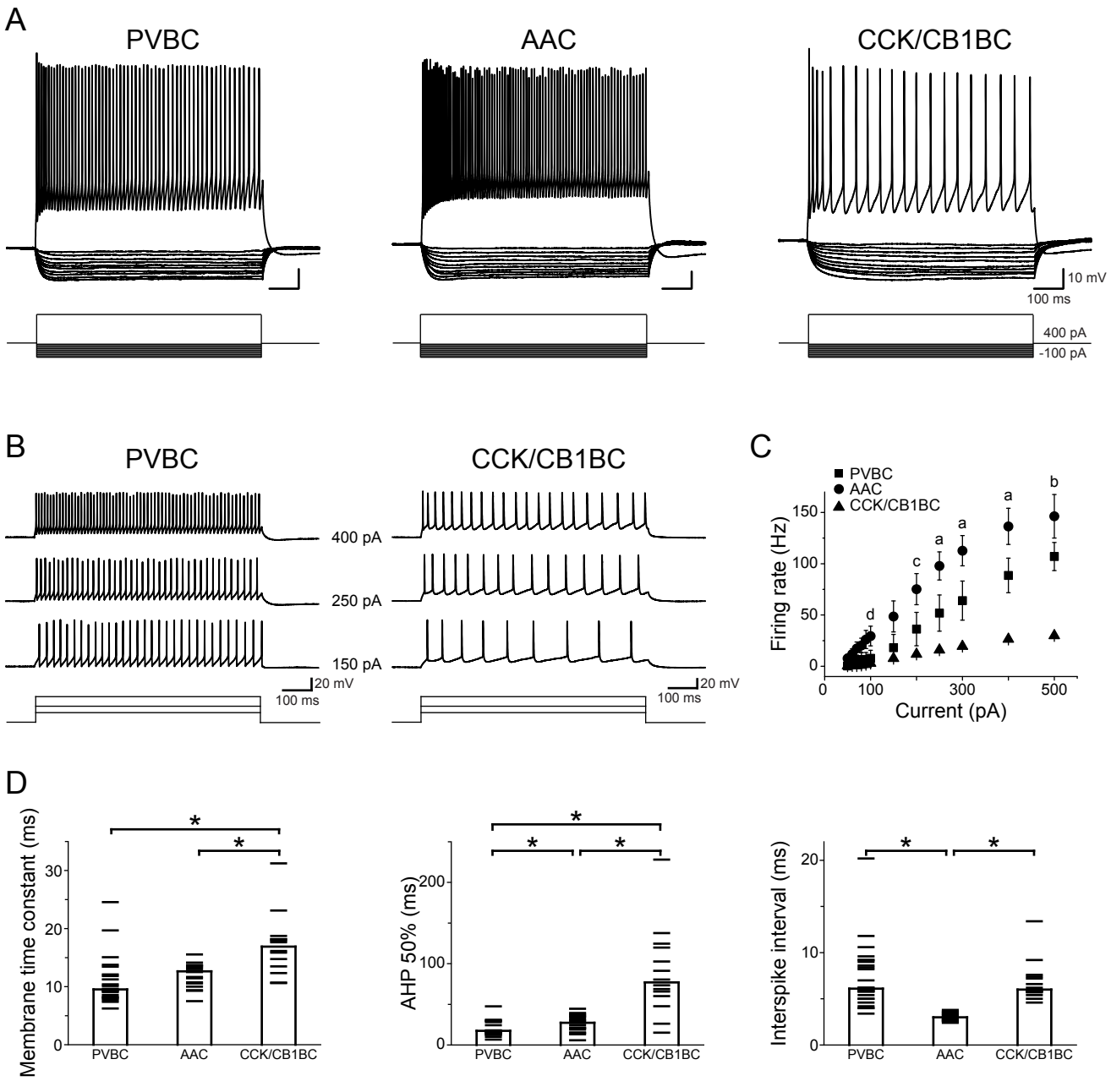
A
PVBC
AAC
CCK/CB1BC
10 mV
100 ms
400 pA
-100 pA
B
PVBC
CCK/CB1BC
400 pA
250 pA
150 pA
20 mV
100 ms
20 mV
100 ms
C
PVBC
AAC
CCK/CB1BC
Firing rate (Hz)
Current (pA)
0
50
100
150
0
100
300
500
a
b
c
d
D
Membrane time constant (ms)
AHP 50% (ms)
Interspike interval (ms)
PVBC
AAC
CCK/CB1BC
*

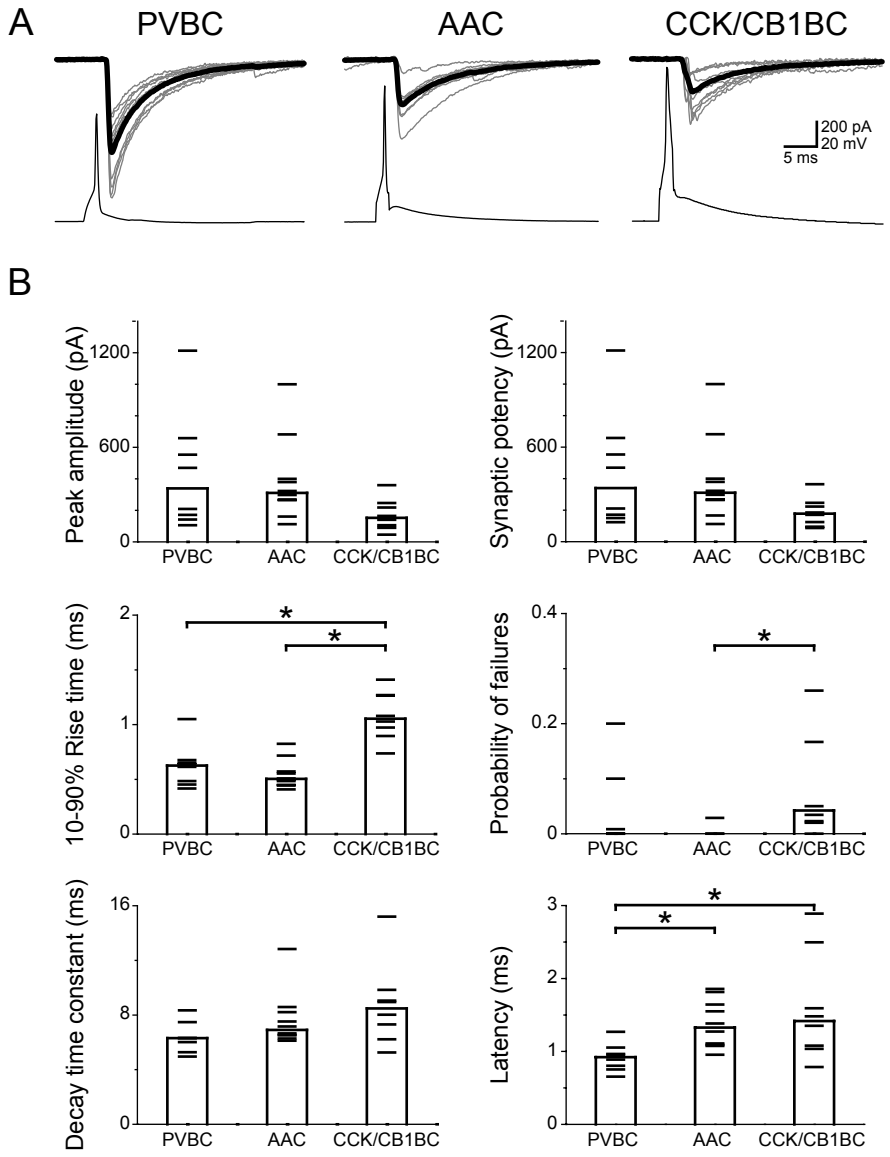
A
PVBC
AAC
CCK/CB1BC
200 pA
20 mV
5 ms
B
Peak amplitude (pA)
1200
600
0
PVBC
AAC
CCK/CB1BC
Synaptic potency (pA)
1200
600
0
PVBC
AAC
CCK/CB1BC
10-90% Rise time (ms)
2
1
0
*
*
PVBC
AAC
CCK/CB1BC
Probability of failures
0.4
0.2
0
*
PVBC
AAC
CCK/CB1BC
Decay time constant (ms)
16
8
0
PVBC
AAC
CCK/CB1BC
Latency (ms)
3
2
1
0
*
*
PVBC
AAC
CCK/CB1BC

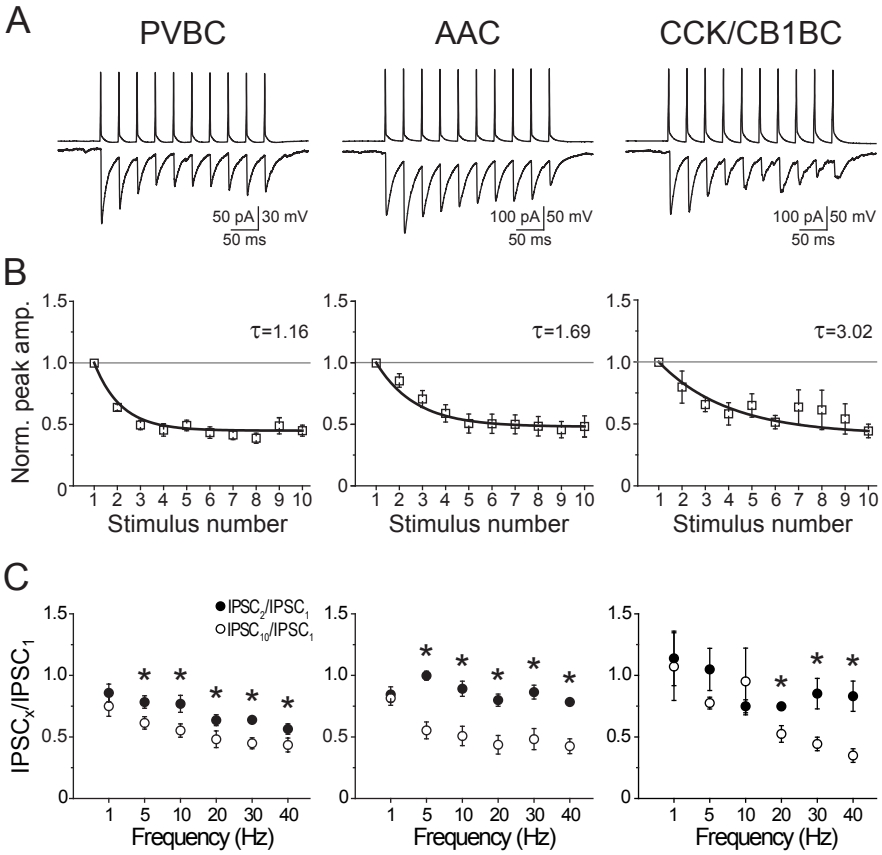
A
PVBC
AAC
CCK/CB1BC
50 pA
30 mV
50 ms
100 pA
50 mV
50 ms
100 pA
50 mV
50 ms
B
Norm. peak amp.
τ=1.16
τ=1.69
τ=3.02
Stimulus number
Stimulus number
Stimulus number
C
IPSC2/IPSC1
IPSC10/IPSC1
IPSCx/IPSC1
Frequency (Hz)
Frequency (Hz)
Frequency (Hz)

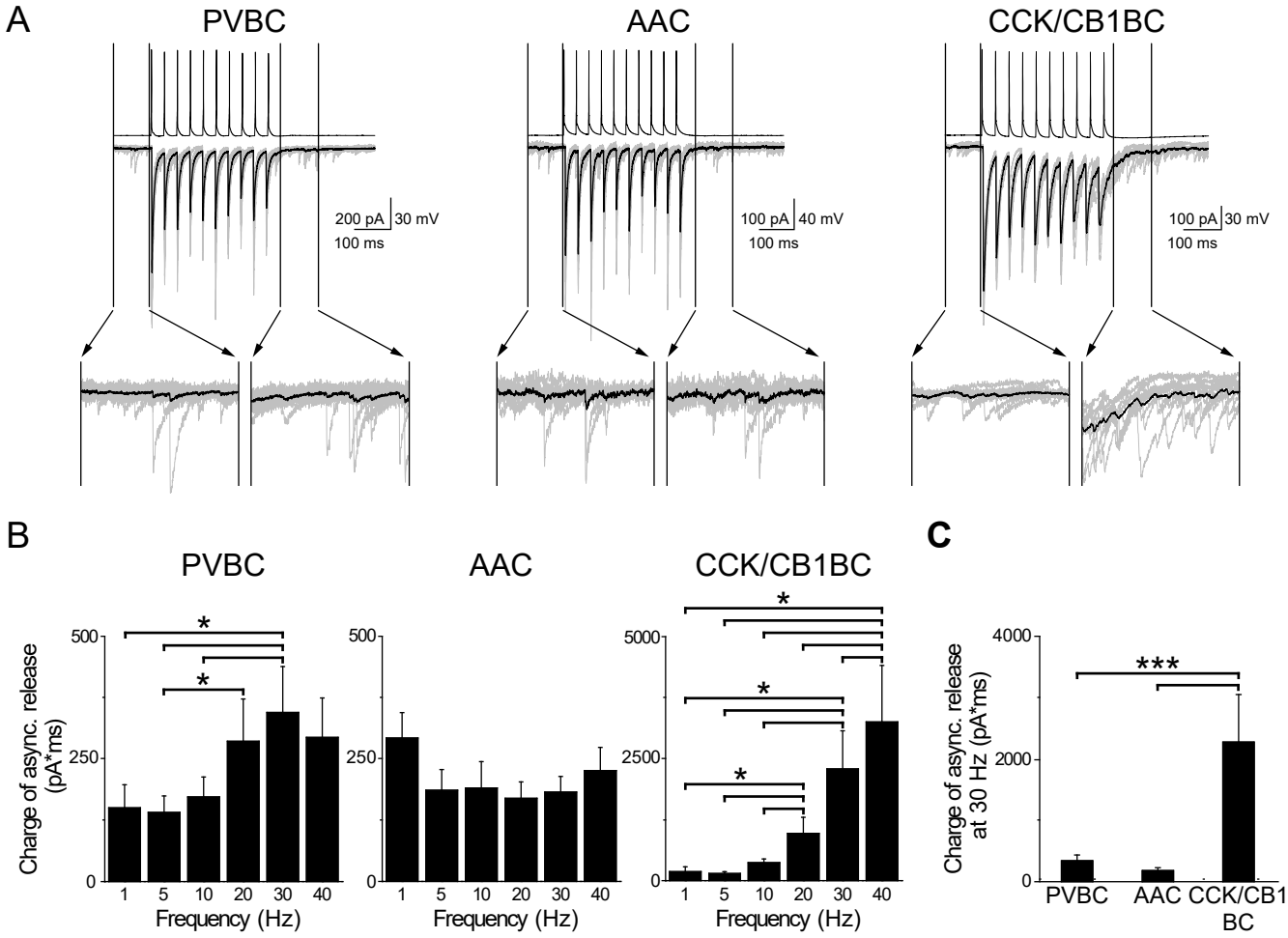
A
PVBC
AAC
CCK/CB1BC
200 pA
30 mV
100 ms
100 pA
40 mV
100 ms
100 pA
30 mV
100 ms
B
PVBC
AAC
CCK/CB1BC
Charge of async. release (pA*ms)
Frequency (Hz)
1
5
10
20
30
40
0
250
500
2500
5000
*
C
Charge of async. release at 30 Hz (pA*ms)
0
2000
4000
***
PVBC
AAC
CCK/CB1 BC